J. Fluid Mech. (2023), *vol*. 962, A26, doi:10.1017/jfm.2023.298

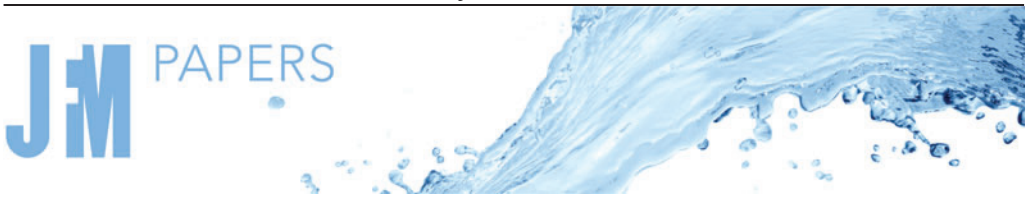

Transient deformation of a viscoelastic capsule in a cross-slot microchannel: effects of inertia and membrane viscosity

R.X. Lu[1], Z.Y. Guo[1], P. Yu[2] and Y. Sui[1],†

[1]School of Engineering and Materials Science, Queen Mary University of London, London E1 4NS, UK

[2]Department of Mechanics and Aerospace Engineering, Southern University of Science and Technology, Shenzhen 518055, PR China

(Received 12 November 2022; revised 10 March 2023; accepted 3 April 2023)

With an immersed-boundary lattice-Boltzmann method, we consider the transit of a three-dimensional initially spherical capsule with a viscoelastic membrane through a cross-slot microchannel. The capsule is released with a small initial off-centre distance in the feeding channel, to mimic experiments where capsules or cells are not perfectly aligned with the centreline. Our main objective is to establish the phase diagram of the capsule's deformation modes as a function of the flow inertia and capsule membrane viscosity. We mainly find three deformation modes in the channel cross-slot. For a capsule with low membrane viscosity, a quasi-steady mode occurs at low Reynolds numbers (*Re*), in which the capsule can reach and maintain a steady ellipsoidal shape near the stagnation point, for a considerable time period. With *Re* increasing to 20, an overshoot–retract mode is observed. The capsule deformation oscillates on an inertial–elastic time scale, suggesting that the dynamics is mainly driven by the balance of the inertial and membrane elastic forces. The membrane viscosity slows down the capsule deformation and suppresses the overshoot–retract mode. A capsule with high membrane viscosity undergoes a continuous-elongation mode, in which its deformation keeps increasing during most of its journey in the channel cross-slot. We summarise the results in phase diagrams, and propose a scaling model which can predict the deformation modes of a viscoelastic capsule in the inertial flow regime. We also discuss implications of the present findings for practical experiments for mechanical characterisation of capsules or cells.

Key words: capsule/cell dynamics, microfluidics

† Email address for correspondence: y.sui@qmul.ac.uk

1. Introduction

Cross-slot microchannels may be employed to generate an extensional flow with a stagnation point at the centre of the cross-slot region. Such flow platforms have been widely used to deform flexible microparticles, such as artificial capsules (de Loubens *et al.* 2014, 2015; Maleki *et al.* 2021) or biological cells (Gossett *et al.* 2012; Guillou *et al.* 2016; Armistead *et al.* 2019), to probe their mechanical properties. In the experiments, the flexible particles often need to be aligned with the centreline of the feeding channel, through hydrodynamic approaches such as inertial (Di Carlo *et al.* 2007) or sheath-flow focusing (Watkins *et al.* 2009), so that they can reach the close proximity of the stagnation point. There, the particle is elongated by the extensional flow into an ellipsoidal shape, with its major axis aligning with the direction of the principal strain.

The deformation of an initially spherical microcapsule in a channel cross-slot can be determined by a number of factors, including the capsule's mechanical properties, its size relative to the channel dimension and initial position in the feeding channel, the viscosity of the channel fluid, the flow strain rate and inertia. Extensive studies, with experimental (Chang & Olbricht 1993; de Loubens *et al.* 2014, 2015; Maleki *et al.* 2021), theoretical (Barthès-Biesel & Sgaier 1985) or numerical (Dodson & Dimitrakopoulos 2008, 2009; Dimitrakopoulos 2014) approaches, have been conducted for the deformation of a capsule trapped at the stagnation point of a planar extension flow, in the Stokes flow regime. The research has systematically considered the effects of the capsule's size and membrane constitutive law, the viscosity contrast between the fluids inside and outside the capsule and the flow strain rate on the capsule's steady deformation. Once the relation is established, one can use the steady capsule profile and flow parameters measured in experiments to inversely infer the mechanical properties of the capsule (de Loubens *et al.* 2015; Maleki *et al.* 2021).

In practical flow experiments, however, it is very difficult to perfectly align microparticles to a desired position. In cross-slot microchannels, capsules or cells are often slightly off centre before entering the cross-slot region. This imperfection in fact allows these flexible particles to flow through the cross-slot within a short time period, enabling one-by-one processing of a large number of particles. With a flow speed reaching $\sim 1\,\mathrm{m\,s^{-1}}$, Gossett *et al.* (2012) operated a cross-slot microchannel in the inertial flow regime and characterised the stiffness of cells with a throughput rate of 2000 cells per second. This is faster than classical approaches, such as atomic force microscopy or micropipette aspiration, by several orders of magnitude.

However, from the fundamental point of view, the transient deformation of initially off-centred capsules or cells flowing through the channel cross-slot region remains poorly understood. In particular, the effects of the initial off-centre distance of a capsule in the feeding channel, the flow inertia and the capsule's membrane viscosity have not been systematically studied. On the other hand, the membrane viscosity of artificial capsules (Chang & Olbricht 1993; Walter, Rehage & Leonhard 2000; Diaz, Barthès-Biesel & Pelekasis 2001) or biological cells (Fischer 1980; Tran-Son-Tay, Sutera & Rao 1984; Evans & Yeung 1989) has been considered in other flow set-ups, and been shown to play important roles in the transient deformation of these flexible particles (Barthès-Biesel & Sgaier 1985; Yazdani & Bagchi 2013; Cordasco & Bagchi 2017; Guglietta *et al.* 2020; Li & Zhang 2021).

In the present study, we consider the transit of an initially spherical capsule with a viscoelastic membrane through a cross-slot microchannel, by means of a well-tested three-dimensional immersed-boundary lattice-Boltzmann method (LBM) (Wang *et al.* 2016; Lu *et al.* 2021). The capsule is released in the feeding channel with a small

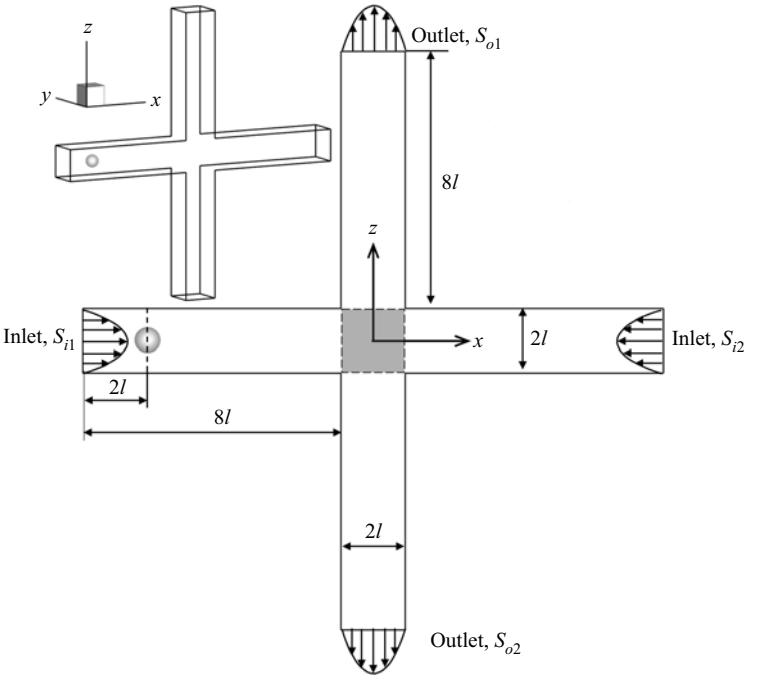

Figure 1. Geometry of the cross-slot channel. The shadow represents the cross-slot region. Top left inset is the three-dimensional view.

initial off-centre distance, to mimic the experimental situation that capsules or cells are imperfectly aligned. We mainly focus on the effects of the flow inertia and capsule membrane viscosity on the capsule's transient deformation in the channel cross-slot, with an aim of establishing a phase diagram of the capsule's deformation modes as a function of these parameters. To the best of our knowledge, it is the first three-dimensional computational study of its kind.

The paper is organised as follows: the flow geometry, governing equations and main dimensionless parameters are detailed in § 2; the numerical method and mesh convergence study are presented in § 3. The simulation results of the effects of the initial off-centre distance, flow inertia and capsule membrane viscosity are presented in § 4. We propose a scaling model to predict the deformation modes of a viscoelastic capsule in the inertial flow regime, and discuss practical implications of the present findings in § 5. We then conclude the paper in § 6.

2. Problem statement

As shown in figure 1, we consider an initially spherical capsule with radius a flowing through a cross-slot microchannel. The four inflow and outflow channel branches all have a constant square cross-section with a side length of $2l$, and a channel length of $8l$. A three-dimensional Cartesian coordinate system is used with the x- and z-directions along the axes of the inflow and outflow channels, respectively, and $x = y = z = 0$ at the centre of the cross-slot region. The fluid motion is governed by the Navier–Stokes equations and the no-slip boundary condition is imposed at the channel walls. At the channel inlets S_{i1}, S_{i2} and outlets S_{o1}, S_{o2}, the fluid velocity profiles are set as the fully developed channel flow with the same flow rate Q. The detailed velocity profiles can be found from

Pozrikidis & Jankowski (1997) and Hu, Salsac & Barthès-Biesel (2012). The present set-up corresponds to experiments where the flow rates are controlled by multiple syringe pumps.

The capsule is enclosed by a viscoelastic membrane with a small bending stiffness. The interior and suspending fluids are both incompressible Newtonian liquids with identical viscosity μ and density ρ. The capsule is released in an inflow channel from the cross-section S_c, which is $2l$ from the inlet S_{i1}. There is a small initial off-centre distance d_{oc} along the $-z$ direction, to mimic the experimental situation where a capsule is not perfectly aligned with the centreline of the feeding channel.

For the viscoelastic membrane of the capsule, the total membrane stress $\boldsymbol{\tau}$ is assumed to be the sum of the elastic and viscous stresses

$$\boldsymbol{\tau} = \boldsymbol{\tau}^e + \boldsymbol{\tau}^v. \tag{2.1}$$

The membrane elasticity is governed by the strain-hardening Skalak law (Skalak *et al.* 1973), which has a strain energy function

$$W = \frac{G_s}{4}\left[\left(I_1^2 + 2I_1 - 2I_2\right) + CI_2^2\right], \tag{2.2}$$

where W is the strain energy density per unit undeformed surface area and G_s is the surface shear elasticity modulus; I_1 and I_2 are the strain invariants of the Green's strain tensor

$$\boldsymbol{E} = \tfrac{1}{2}\left(\boldsymbol{F}^{\mathrm{T}} \cdot \boldsymbol{F} - \boldsymbol{I}\right), \tag{2.3}$$

where $\boldsymbol{F} = \partial \boldsymbol{x}/\partial \boldsymbol{X}$ is the deformation gradient of the deformed capsule configuration $\boldsymbol{x}$ with respect to the undeformed configuration $\boldsymbol{X}$; I_1 and I_2 are defined as $I_1 = {\lambda_1}^2 + {\lambda_2}^2 - 2, I_2 = (\lambda_1\lambda_2)^2 - 1$, where λ_1, λ_2 are the two principal extension ratios. The term C is a constant and is related to the membrane area dilatation modulus K_s by $K_s = (1 + 2C)G_s$. We set $C = 1$ in the present study.

The elastic stress tensor $\boldsymbol{\tau}^e$ can be obtained from

$$\boldsymbol{\tau}^e = \tau_1^e \boldsymbol{e}_1 \otimes \boldsymbol{e}_1 + \tau_2^e \boldsymbol{e}_2 \otimes \boldsymbol{e}_2, \tag{2.4}$$

where

$$\tau_1^e = \frac{1}{\lambda_2}\frac{\partial W}{\partial \lambda_1}, \quad \tau_2^e = \frac{1}{\lambda_1}\frac{\partial W}{\partial \lambda_2}, \tag{2.5a,b}$$

are the two principal stresses and $\boldsymbol{e}_1, \boldsymbol{e}_2$ are their corresponding directions, which can be obtained from the unit eigenvectors of the left Cauchy–Green deformation tensor $\boldsymbol{G} = \boldsymbol{F} \cdot \boldsymbol{F}^{\mathrm{T}}$.

The membrane viscous stress $\boldsymbol{\tau}^v$ has contributions from the shear viscosity μ_s and area dilatational viscosity μ_s' (Barthès-Biesel & Sgaier 1985)

$$\boldsymbol{\tau}^v = \mu_s[2\boldsymbol{D} - \mathrm{tr}(\boldsymbol{D})\boldsymbol{P}] + \mu_s' \,\mathrm{tr}(\boldsymbol{D})\boldsymbol{P}, \tag{2.6}$$

where $\boldsymbol{D}$ is the membrane strain rate tensor, $\mathrm{tr}(\boldsymbol{D})$ is the area dilatation rate and $\boldsymbol{P} = \boldsymbol{I} - \boldsymbol{nn}$ is the projection tensor of the deformed membrane, with $\boldsymbol{n}$ as the unit normal vector. In the present study, we set $\mu_s' = 3\mu_s$, so that the relaxation times corresponding to the membrane shear and dilatational viscosity are equal (i.e. $\mu_s/G_s = \mu_s'/K_s$).

The bending resistance of the membrane is modelled using Helfrich's formulation (Zhong-Can & Helfrich 1989)

$$E_b = \frac{k_c}{2}\int_A (2H - c_0)^2 \,\mathrm{d}A, \tag{2.7}$$

where k_c is the bending modulus, H is the mean curvature, c_0 is the spontaneous curvature and A is the surface area. A small bending stiffness $k_c = 0.004G_s a^2$ is used in the present

study to prevent the formation of membrane wrinkles. We set c_0 as zero. The bending force density derived from the bending energy formulation is (Zhong-Can & Helfrich 1989; Guckenberger & Gekle 2017)

$$\boldsymbol{f_b} = k_c \left[2H(2H^2 - 2\kappa_g) + \nabla_s \cdot \nabla_s (2H) \right] \boldsymbol{n}, \tag{2.8}$$

where κ_g is the Gaussian curvature.

The present problem is governed by the following dimensionless parameters:

(i) the flow Reynolds number $Re = 2\rho Ul/\mu$, where U is the average flow speed in the inflow/outflow channels;
(ii) the capillary number $Ca = \mu U/G_s$, which measures the relative importance of the fluid viscous and membrane elastic forces;
(iii) the dimensionless capsule membrane viscosity $\eta = \mu_s/\mu a$;
(iv) the capsule confinement ratio a/l, which compares the size of the capsule relative with the channel; and
(v) the dimensionless initial off-centre distance d_{oc}/l.

We are mainly interested in the capsule deformation in the channel cross-slot region ($-l \leq x, y, z \leq l$, shown in figure 1), where the capsule is elongated into an ellipsoidal shape. We quantify its deformation using the Taylor deformation parameter

$$D_{XZ} = \frac{a_3 - a_1}{a_3 + a_1}, \tag{2.9}$$

where a_1 and a_3 are the maximum dimensions of the capsule along the x- and z-axes, respectively, in the symmetric $y = 0$ plane.

3. Numerical method

The present study is based on an immersed-boundary LBM that has been verified extensively for a capsule with a hyperelastic or viscoelastic membrane in shear or channel flows (Sui *et al.* 2008; Wang *et al.* 2016, 2018; Lu *et al.* 2021; Lin *et al.* 2021). Here, we only provide a brief introduction. The fluid domain is governed by the Navier–Stokes equations that are solved by a three-dimensional nineteen-velocity LBM with a grid size of $\Delta x = \Delta y = \Delta z = 2l/80$. The no-slip boundary condition at the walls is implemented by a second-order bounce-back scheme (Bouzidi, Firdaouss & Lallemand 2001). At the channel inlets and outlets, the velocity boundary conditions are implemented with a second-order non-equilibrium extrapolation method (Guo, Zheng & Shi 2002).

The interaction between the fluid and capsule is solved by an immersed-boundary method (Peskin 2002). The capsule membrane is discretised into 8192 flat triangular face elements, which are connected with 4098 nodes, following Ramanujan & Pozrikidis (1998). In the immersed-boundary method, the no-slip boundary condition at the capsule membrane is satisfied by letting the membrane move at the same velocity as the fluid around it. Since the membrane area is not conserved, the capsule will deform from its initial spherical shape. For the membrane viscoelastic stress, previous studies have shown that directly solving (2.1) leads to numerical instabilities (Yazdani & Bagchi 2013; Li & Zhang 2019). Here, we follow the method of Yazdani & Bagchi (2013) where a slightly modified mechanical system is employed to approximate equation (2.1). Details of the implementation can be found in Yazdani & Bagchi (2013) and pertinent literature (Holzapfel 2000; ABAQUS/Standard Theory Manual 2002). To calculate the membrane bending force in (2.8), a quadratic surface fit has been used to evaluate the curvatures and

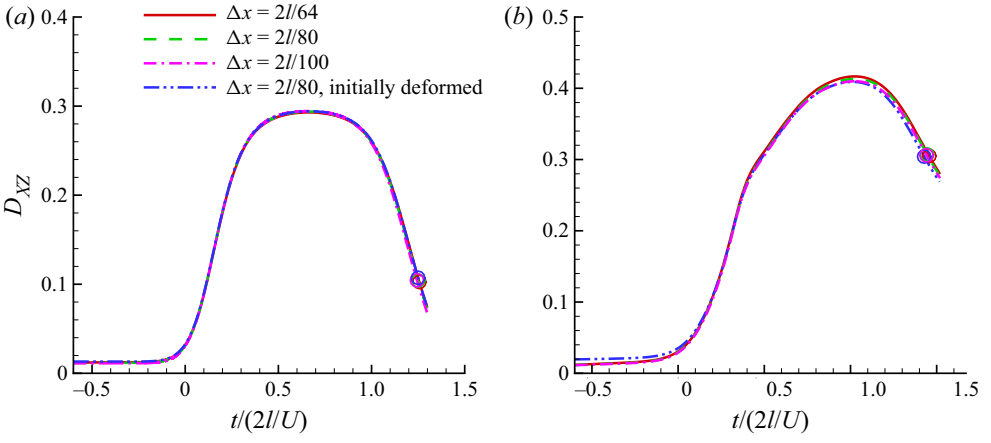

Figure 2. Effects of the LBM mesh size and capsule's initial deformation on the time evolution of the Taylor deformation parameter D_{XZ} of a capsule with $a/l = 0.4$ and $d_{oc} = 0.02l$. At $t = 0$ the capsule starts to enter the cross-slot region; the circle symbols mark the moments when the capsule completely leaves the region. Other parameters are: (*a*) $Re = 1$, $Ca = 0.1$ and $\eta = 0$; (*b*) $Re = 80$, $Ca = 0.1$ and $\eta = 40$.

normal direction at each membrane node, following the approaches of Garimella & Swartz (2003) and Yazdani & Bagchi (2012).

Since the present numerical method has been well tested previously, here, we evaluate the effect of the LBM grid size on the transient deformation of capsules with a hyperelastic or viscoelastic membrane and $a/l = 0.4$, $d_{oc} = 0.02l$, in both viscous and inertial flow regimes. Three mesh resolutions $\Delta x = 2l/64$, $2l/80$ and $2l/100$ have been tested, and the time evolutions of the Taylor deformation parameter D_{XZ} are presented in figure 2. In all figures of the present study on the time evolution of D_{XZ}, we set $t = 0$ as the time when a capsule starts to enter the cross-slot region, i.e. any membrane element reaches the plane $x = -l$. We use a circle symbol to mark the time when the entire capsule leaves the cross-slot. From figure 2, we can see that the time evolutions of D_{XZ} almost superimpose for all three flow meshes. We also test the effect of membrane mesh size, and find that increasing the number of membrane elements to 32 768 does not lead to any visible change to the results. In all simulations, the volume change of the capsule is within 0.2 %. The capsule also remains symmetric approximately along the $y = 0$ plane, with the deviation between the capsule's mass centre and the $y = 0$ plane less than $1 \times 10^{-5}l$.

With the present computational domain, a capsule with a highly viscous membrane (i.e. $\eta \geq 40$) cannot reach its steady deformation in the feeding channel. It is therefore interesting to check how this will affect the capsule's transient deformation in the channel cross-slot. With the same parameters of figure 2, we consider capsules that are already in steady deformed shapes when released from S_c, to mimic the situation that the feeding channel is long enough for the capsules to reach their steady deformation. The time evolutions of D_{XZ} are added to figure 2. The results suggest that the capsule deformation in the cross-slot region is little affected by the initial deformation state.

4. Results

4.1. *Effect of the initial off-centre distance d_{oc}*

In practical experiments, it is always crucial to align capsules or biological cells to the centreline of the feeding channel, so that these flexible particles can reach the close

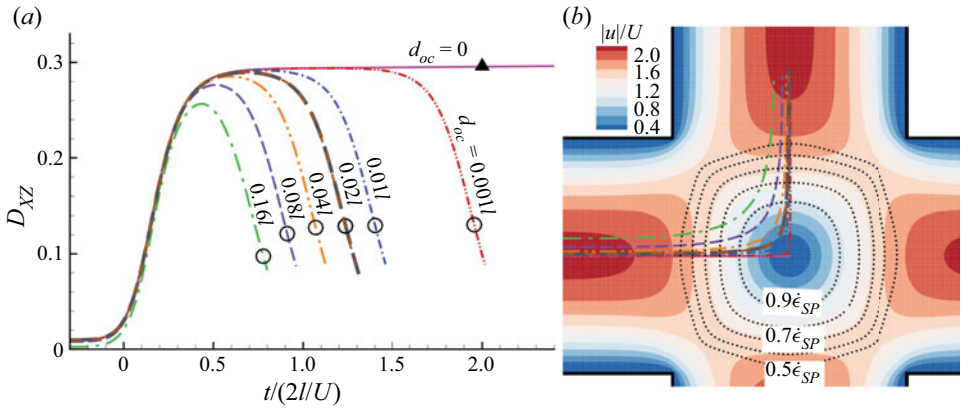

Figure 3. (*a*) Effect of the initial off-centre distance d_{oc} on the time evolution of the Taylor deformation parameter D_{XZ} of a capsule with $a/l = 0.4$, $\eta = 0$ at $Re = 1$, $Ca = 0.1$. The triangle symbol marks D_S, the steady D_{XZ} of the same capsule released at the stagnation point. The thick long dashed line is the result of a capsule with an initial offset of $0.02l$ in both the $-y$ and $-z$ directions. (*b*) Velocity magnitude $|u|$ (colour contour) of the unperturbed background flow of (*a*) in the plane $y = 0$. Dotted lines are the strain rate. The maximum strain rate appears at the stagnation point and is represented by $\dot{\epsilon}_{sp}$. Trajectories of the mass centre of the capsule of (*a*) are also presented in (*b*), using lines with the same legend as (*a*).

proximity of the stagnation point, where their maximum deformation is recorded and then fitted to theoretical or computational model predictions, to inversely infer the particles' mechanical properties (Armistead *et al.* 2019; Maleki *et al.* 2021). Often, these models only consider particles that are centrally aligned. Significantly off-centred particles experience different levels of fluid stresses and their maximum deformation in the cross-slot region can be much smaller than that of centrally aligned particles (Hymel, Lan & Khismatullin 2020). In the present study, it is therefore important that we first consider the effect of the initial off-centre distance, and establish the threshold d_{oc}, below which the capsule can be considered as well aligned.

We conduct the test by considering the effect of the initial off-centre distance on the transient deformation of a capsule with $a/l = 0.4$, $\eta = 0$ at $Re = 1$, $Ca = 0.1$. The capsule is released from different initial off-centre positions with $0 \leq d_{oc} \leq 0.16l$ in the $-z$ direction. The time evolutions of the Taylor shape parameter D_{XZ}, and the trajectories of the capsule's mass centre are presented in figures 3(*a*) and 3(*b*), respectively. We can see that a perfectly aligned capsule ($d_{oc} = 0$) reaches steady deformation and stays in close proximity to the stagnation point. The steady D_{XZ} is identical to D_S, marked by the triangle in figure 3(*a*), which represents the steady Taylor deformation parameter of the same capsule initially released at the stagnation point. Note that this is in fact an unstable state, and the numerical error in the computational simulation will eventually cause the capsule to depart from the channel centreline and flow out of the cross-slot region. However, for the time scale considered in the present study, until $t/(2l/U) = 2.5$, the offset of the capsule's mass centre from $z = 0$ remains extremely small, i.e. less than $4 \times 10^{-5}l$. With d_{oc} increasing, but remaining small, i.e. $d_{oc} < 0.04l$, the capsule can reach a quasi-steady state when it is near the stagnation point, and the quasi-steady D_{XZ} is comparable to D_S (see figure 3*a*). The time period that the capsule stays in the quasi-steady state is of the order of $2l/U$, and decreases with d_{oc}. Further increasing the initial off-centre distance to $d_{oc} \geq 0.04l$, the quasi-steady state can no longer be observed. The capsule reaches its maximum deformation when getting closest to the stagnation point, with the peak D_{XZ}

being considerably smaller than D_S, and then the Taylor deformation parameter drops quickly as the capsule leaves the stagnation point.

We also consider the effect of a small initial off-centre distance along the $-y$ direction and an example is presented in figure 3(a), for a capsule with an initial off-centre distance of $0.02l$ along both the $-y$ and $-z$ directions. The result is visually identical to that of the capsule with a $0.02l$ offset only in the $-z$ direction, suggesting that a small initial offset along the $-y$ direction has negligible effect on the capsule deformation.

The results of figure 3(a) can be understood by examining the unperturbed background flow, which is presented in figure 3(b) for the flow strain rate $\dot{\epsilon}$ and velocity magnitude $|u|$. As expected, the maximum strain rate appears at the stagnation point, which we term as $\dot{\epsilon}_{sp}$. Around the stagnation point, there is a circular region, with a radius of approximately $0.44l$, in which the strain rate slowly decreases with the distance to the stagnation point, but remains very high, i.e. $\dot{\epsilon} \geq 0.9\dot{\epsilon}_{sp}$. Outside the region, $\dot{\epsilon}$ decreases much more quickly with the distance to the stagnation point. The trajectory of a capsule with a larger d_{oc} is generally farther away from the stagnation point, which has two effects. Firstly, the capsule experiences lower fluid stress that varies more rapidly with the distance to the stagnation point; secondly, the capsule travels faster when passing the region near the stagnation point. Both effects contribute to the observation that a quasi-steady state does not exist for a capsule released with a large d_{oc}.

In the present study, we mainly consider capsules with $d_{oc} \sim 0.02l$. With such small initial off-centre distances, a capsule may reach a quasi-steady state at low flow Reynolds numbers, and the quasi-steady deformation could be comparable to the steady deformation of the same capsule released at the stagnation point. The condition could be easier to achieve in experiments, compared with much smaller $d_{oc} \sim 0.001l$, and capsules can flow through the channel cross-slot more quickly, enabling a higher processing throughput rate.

4.2. *Quasi-steady and overshoot–retract deformation of a hyperelastic capsule*

Although experiments of cells flowing through cross-slot microchannels have been regularly conducted in the inertial flow regime, where the flow Reynolds number in the feeding channel can reach ∼100 (Gossett *et al.* 2012; Armistead *et al.* 2019), the transient cell dynamics in the channel cross-slot remains poorly understood. In particular, the effects of flow inertia and cell membrane viscosity on the cell deformation have not been systematically studied.

As a first attempt to understand these effects, in this section, we consider the transient deformation of a capsule enclosed by a hyperelastic membrane in the cross-slot channel with finite inertia. The capsule has a confinement ratio of $a/l = 0.4$ and is released with an initial off-centre distance $d_{oc} = 0.02l$. We fix the properties of the channel fluid and the capsule, so that $Ca/Re = 0.0025$, and the inertial effect is studied by increasing the flow velocity U. With the capillary number Ca increasing from $Ca = 0.0025$ to 0.2, Re increases from 1 to 80.

The time evolutions of the Taylor deformation parameter of the capsule at different flow Reynolds numbers are presented in figure 4(a). When $Re \leq 10$, the capsule can reach a quasi-steady state when it is approaching the stagnation point, and the quasi-steady D_{XZ} is very close to the corresponding D_S, which is the steady Taylor deformation parameter of the same capsule released from the stagnation point. For the two quasi-steady cases in figure 4(a) at $Re = 1$ and 10, since the capsule deformation is small, we also compare the quasi-steady D_{XZ} with the predictions of the small deformation theory of Barthès-Biesel & Sgaier (1985), considering the same capsule in planar extensional flow at $Re = 0$. The differences are within 4 %.

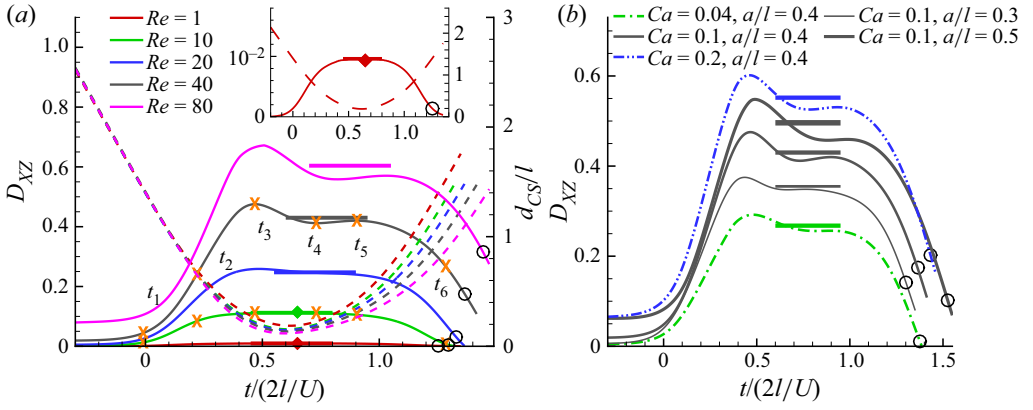

Figure 4. (*a*) Effect of flow inertia on the time evolution of the Taylor deformation parameter (left *y*-axis, solid lines) of a capsule with $a/l = 0.4$, $\eta = 0$ and $Ca/Re = 0.0025$. The horizontal bold lines mark D_S, which is the steady Taylor deformation parameter of the same capsule released from the stagnation point under the same flow condition. The diamond symbols represent the Taylor deformation parameter predicted by the small deformation theory of Barthès-Biesel & Sgaier (1985) for the same capsule in planar extensional flow at $Re = 0$; $t_1, t_2, \ldots, t_6$ are six dimensionless times at -0.01, 0.22, 0.47, 0.72, 0.90 and 1.28, respectively, when the instantaneous capsule profiles will be shown in figure 5. The circle symbols mark the times when the capsule completely leaves the cross-flow region. The dashed lines are the time evolutions of the distance between the capsule's mass centre and the stagnation point d_{CS} (measured by the right *y*-axis). The inset provides a clearer view of the results for the capsule at $Re = 1$. (*b*) Effect of the membrane shear elasticity G_s on the time evolution of the Taylor deformation parameter of a capsule with $a/l = 0.3 \sim 0.5$, $\eta = 0$ at $Re = 40$. Note that $G_s = \mu U/Ca$. The deformation is compared with the corresponding D_S, marked by the horizontal bold solid lines.

To show the transient capsule deformation in the quasi-steady mode, in figure 5(*a*) we present the instantaneous shapes of the capsule at $Re = 10$ at six different time instances. The animation of the capsule deformation can be found from supplementary movie 1 available at https://doi.org/10.1017/jfm.2023.298. It is seen that the capsule profiles are almost identical between t_3 and t_5. In figure 5(*a*), we also present the trajectory of the capsule's mass centre, and use a bold line to highlight the part of the trajectory where the capsule is in the quasi-steady state, i.e. the capsule is approximately at the maximum deformation with $D_{XZ} \geq 0.95 D_{XZ}^{max}$. We can see that the quasi-steady state takes place when the capsule is near the stagnation point.

With the increase of flow inertia, the quasi-steady deformation of the capsule can no longer be observed, as shown in figure 4(*a*) for $Re \geq 20$. Interestingly, we find that, after entering the cross-slot region, the capsule quickly reaches its maximum deformation, with D_{XZ}^{max} being considerably larger than the corresponding D_S, and then D_{XZ} starts to decrease, even when the capsule is still approaching the stagnation point. In general, the time evolution of D_{XZ} shows dampened oscillation. An example of this new deformation mode is presented in figure 5(*b*) for the capsule at $Re = 40$, and the animation is shown in supplementary movie 2. The capsule's elongational deformation overshoots and peaks at t_3, before the capsule's mass centre reaches the closest position to the stagnation point. After t_3, the capsule retracts with D_{XZ} decreasing to a local minimum at t_4, and then the capsule deformation starts to increase again. We name this deformation mode overshoot–retract deformation.

In the overshoot–retract mode, we find that the dimensionless characteristic time scale of the oscillation of D_{XZ}, e.g. $t_4 - t_3 = 0.25$ for the capsule at $Re = 40$, is of the same

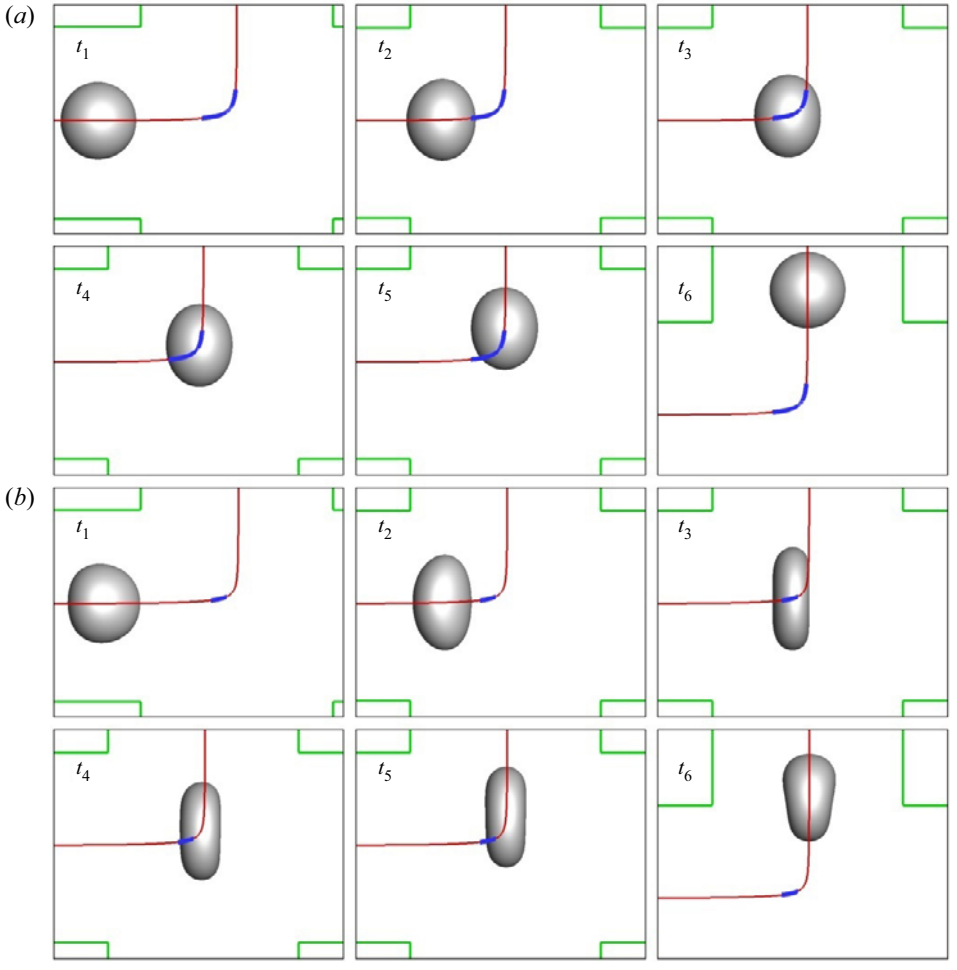

Figure 5. Instantaneous profiles of the capsule of figure 4(*a*) at $Re = (a)$ 10, (*b*) 40. The red solid lines are the trajectories of the capsule's mass centre; the bold blue lines mark the parts of trajectories where the capsule is approximately at the maximum deformation ($D_{XZ} \geq 0.95 D_{XZ}^{max}$). The time instances are provided in figure 4(*a*).

order as the inertial–elastic time

$$t_{ic} = \sqrt{\rho a^3 / G_s} = 0.18. \tag{4.1}$$

The agreement suggests that the oscillation of the capsule deformation is mainly driven by the balance of the flow inertial and membrane elastic forces.

We also consider the effect of the membrane shear elasticity G_s on the transient deformation of the capsule in the inertial flow regime. We present the results in figure 4(*b*) for capsules at $Re = 40$, with different values of G_s that have led to $Ca = 0.04$, 0.1 and 0.2. Note that $G_s = \mu U/Ca$. Besides $a/l = 0.4$, we have also considered capsules with different confinement ratios of 0.3 and 0.5 at $Ca = 0.1$. All cases are in the overshoot–retract deformation mode. The maximum D_{XZ} decreases with G_s but increases with the capsule size, and is always approximately 10 % larger than the corresponding D_S. Interestingly, we find that the average of the values of D_{XZ} at the peak and the

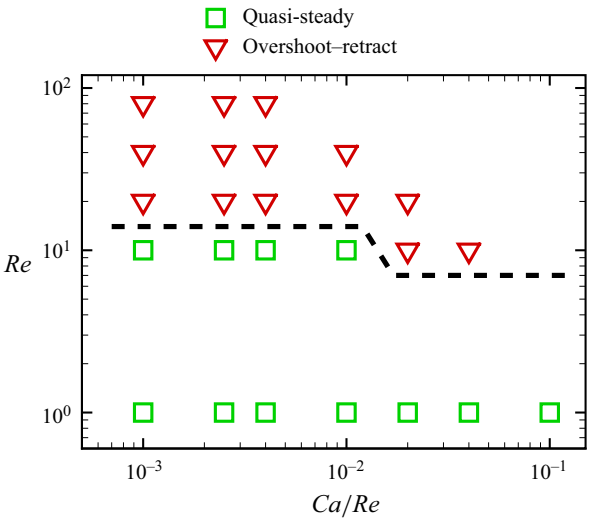

Figure 6. Phase diagram of the deformation modes of a hyperelastic capsule as a function of Re and Ca/Re. The dashed line is the approximate phase boundary.

following trough is only approximately 2 % larger than the corresponding D_S. We will discuss practical implications of this observation in § 5.2.

We conduct extensive simulations for hyperelastic capsules with $a/l = 0.4$ at different (Ca/Re, Re) combinations, and summarise the deformation modes in a phase diagram in figure 6. At $Ca/Re = 0.0025$ and $1 \leq Re \leq 80$, corresponding to figure 4(a), we also consider capsules with different confinement ratios of $a/l = 0.3$ and 0.5. The deformation modes are identical to those of capsules with $a/l = 0.4$. From the phase diagram, it is clear that the quasi-steady mode only prevails when the inertial effect is very weak (e.g. $Re \leq 1$). At high inertia, i.e. $Re \geq 20$, the capsule undergoes the overshoot–retract deformation.

4.3. *Three deformation modes of a viscoelastic capsule*

In this section, we focus on the effect of the membrane viscosity on the transient deformation of a capsule in the channel cross-slot region. We use the capsule of figure 5(b) at $Re = 40$, $Ca = 0.1$ as the baseline case and increase the membrane viscosity η from 0 to 40. Note that the range of η considered here is relevant to practical experiments. For artificial capsules with a nylon or human serum albumin membrane, $\eta \sim 6$ and 12, respectively, in the previous experiments of Chang & Olbricht (1993), Diaz *et al.* (2001) and Gires *et al.* (2016). The membrane viscosity of human red blood cells measured in experiments can range from 10^{-7} to $10^{-6}\,\mathrm{N\,s\,m^{-1}}$ (Evans & Hochmuth 1976; Hochmuth, Worthy & Evans 1979; Tran-Son-Tay *et al.* 1984). If one operates experiments using a liquid with $\mu = 0.01\,\mathrm{Pa\,s}$, and we assume the equivalent radius of a red blood cell is $3\,\mu\mathrm{m}$, the dimensionless membrane viscosity will be $3.3 \leq \eta \leq 33$. Granulocytes have been found to have a higher membrane viscosity, of the order of $10^{-5}\,\mathrm{N\,s\,m^{-1}}$, which could lead to $\eta \sim 100$.

The time evolutions of the Taylor deformation parameter of the capsule with increasing η are presented in figure 7(a). It is clear from the results that the membrane viscosity tends to slow down the capsule deformation and smooth the overshoot–retract deformation in the inertial flow regime. At $\eta = 5$, the overshoot–retract mode has disappeared and the capsule deformation is in the quasi-steady mode. The quasi-steady D_{XZ} is still comparable

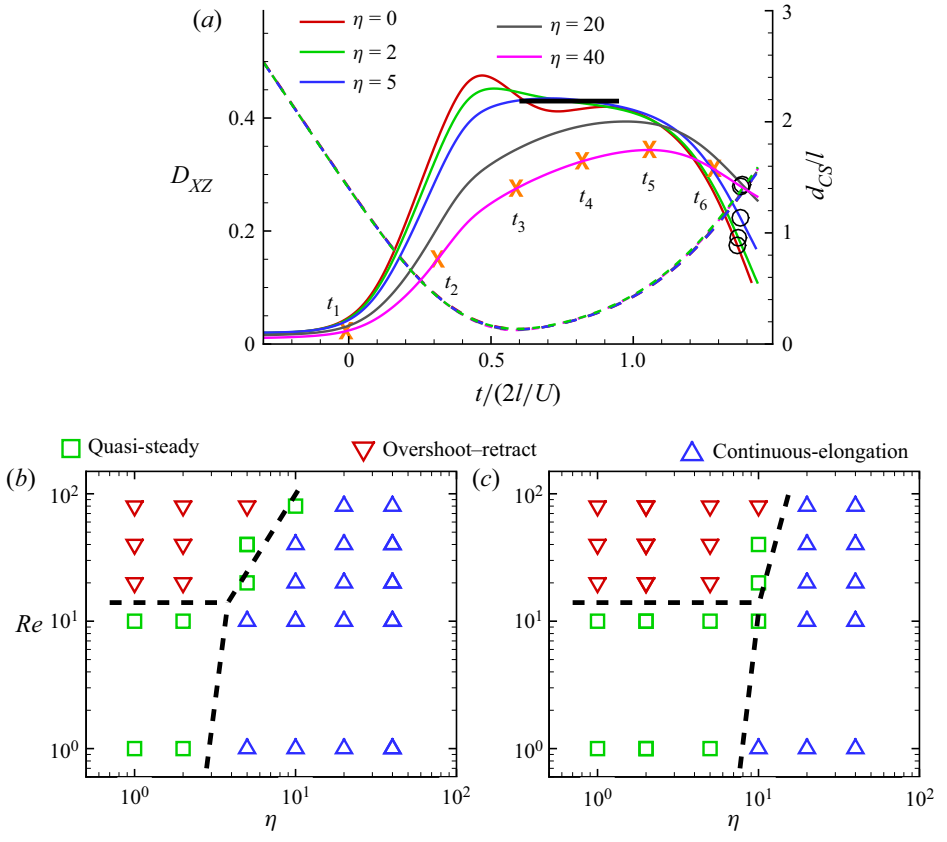

Figure 7. (*a*) Effect of membrane viscosity on the time evolution of the Taylor deformation parameter (left *y*-axis, solid lines) of a capsule with $a/l = 0.4$ at $Re = 40$ and $Ca = 0.1$. The horizontal bold line marks D_S; $t_1, t_2, \ldots, t_6$ are six dimensionless times at -0.01, 0.31, 0.59, 0.82, 1.06 and 1.28, respectively, when the instantaneous capsule profiles are shown in figure 8. The circle symbols mark the times when the capsule leaves the cross-slot region. The dashed lines are the time evolution of the distance between the capsule's mass centre and the stagnation point d_{CS} (the right *y*-axis). (*b*,*c*) Phase diagram of the capsule's deformation modes depending on the membrane viscosity and flow inertia at $Ca =$ (*b*) 0.1, (*c*) 0.04. Dashed lines are the approximate phase boundaries.

to the corresponding D_S. It should be noted that all capsules considered in figure 7(*a*) share the same D_S, since the steady deformation of the capsules in the extensional flow is unaffected by the capsules' membrane viscosity.

As η continues to increase, a new deformation mode emerges, which we present in figure 8 for the instantaneous shapes of the capsule of figure 7(*a*) with $\eta = 40$. The animation of the transient deformation is shown in supplementary movie 3. A salient feature of the new mode is that the capsule deformation keeps increasing, even when the capsule has left the stagnation point and is approaching the exit of the channel cross-slot. We thus name this deformation pattern the continuous-elongation mode. With $\eta = 40$, the Taylor shape parameter of the capsule during its entire journey in the channel cross-slot is considerably smaller than D_S. From figure 7(*a*), we also notice that the membrane viscosity has little effect on the time evolution of d_{CS}, which suggests that the capsule's trajectory is not sensitive to its membrane viscosity.

At $Ca = 0.1$ for capsules with $a/l = 0.4$ and $\eta = 0$–40, we vary the flow Reynolds number from 1 to 80, and present the phase diagram of the capsule deformation modes

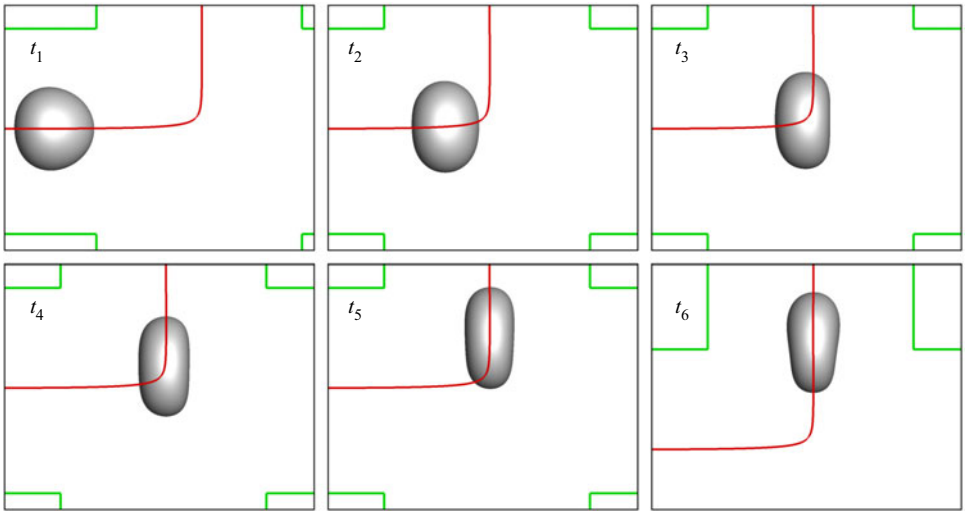

Figure 8. Instantaneous profiles of the capsule of figure 7(*a*) with $\eta = 40$. The red solid line is the trajectory of the capsule's mass centre. The six time instances are provided in figure 7(*a*).

as a function of the membrane viscosity and flow Reynolds number in figure 7(*b*). At $Re = 1$ and 40, and $0 \leq \eta \leq 40$, we also consider capsules with different confinement ratios of a/l =0.3 and 0.5. The deformation modes are identical to those of capsules with a/l =0.4 and are therefore not shown in the phase diagram. We find that capsules with low membrane viscosity (i.e. $\eta \leq 2$) respond to the flow like a hyperelastic capsule, with the deformation transiting from the quasi-steady to overshoot–retract mode with Re increasing. For capsules with a highly viscous membrane, i.e. $\eta \geq 10$, the continuous-elongation mode becomes the dominant mode of capsule deformation. In the inertial flow regime ($Re \geq 20$), the transition from the overshoot–retract to continuous-elongation mode due to an increase of η happens via the quasi-steady mode. At higher Re, larger membrane viscosity is needed for this transition to take place. We will further discuss the transition in the following § 5.1. We also consider stiffer capsules with all other parameters the same as those of figure 7(*b*), and the phase diagram for $Ca = 0.04$ is presented in figure 7(*c*). A noticeable difference, compared with figure 7(*b*), is that the threshold η for the continuous-elongation mode has increased, which suggests that a stiffer membrane promotes the quasi-steady and overshoot–retract modes for viscoelastic capsules.

With $d_{oc} = 0.01l$ and all other parameters remaining the same as those of figure 7(*b*), we conduct simulations to test the effect of a smaller initial off-centre distance on the capsule's deformation phase diagram. We find that the phase diagram remains unchanged.

5. Discussion

5.1. *A scaling model for capsule deformation in inertial flow regime*

We propose a scaling model to predict the deformation mode of a capsule in the inertial flow regime at $Re \geq 20$. In this model, we assert that a capsule's deformation mode is mainly determined by the competition of the inertial–elastic time scale $t_{ic} = \sqrt{\rho a^3/G_s}$ and the membrane viscosity time scale $t_{mv} = \mu_s/G_s$, which are associated with the overshoot–retract and continuous-elongation modes, respectively. The capsule will adopt

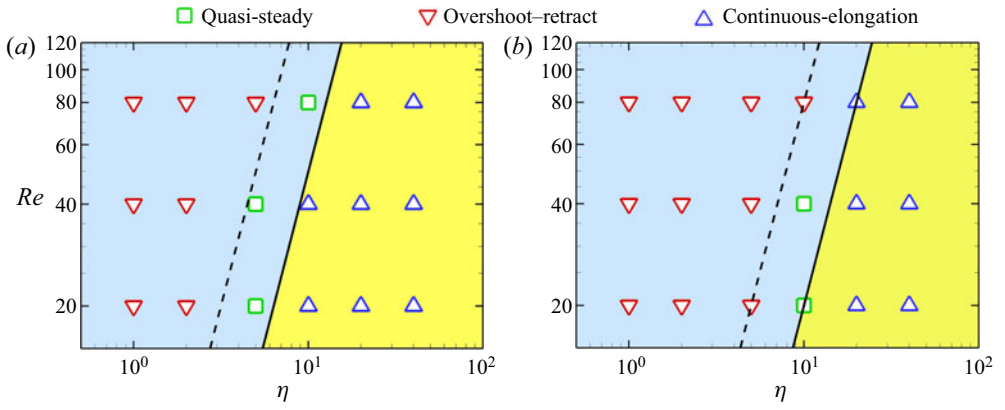

Figure 9. Comparison of the predictions using the scaling model with the phase diagram of figure 7(*b*,*c*) at $Re \geq 20$ and $Ca =$ (*a*) 0.1, (*b*) 0.04. Symbols are obtained from direct numerical simulations. The light blue and yellow regions are the scaling model-predicted parametric space for the overshoot–retract and continuous-elongation modes, respectively. The solid lines are the scaling model-predicted phase boundaries at which $t_{mv} = t_{ic}$ (or $\eta \cdot Oh = 1$), the dashed lines mark the (η, Re) combination at which $\eta \cdot Oh = 0.5$.

the mode associated with the longer time scale, and the transition between the two modes will take place when the two time scales are comparable, i.e. $t_{mv}/t_{ic} \sim 1$.

We test the scaling model by predicting the phase diagrams of figure 7(*b*,*c*) for $Re \geq 20$, and the results are shown in figures 9(*a*) and 9(*b*), respectively. In the figures, the solid lines mark the (η, Re) combination at which $t_{mv} = t_{ic}$. In the light blue regions, $t_{ic} > t_{mv}$, and a capsule should be largely in the overshoot–retract mode according to the model. While in the yellow regions, $t_{mv} > t_{ic}$, the deformation of a capsule is predicted to be the continuous-elongation mode. Our model seems to predict the phase diagram of capsule deformation reasonably well.

Interestingly, when $t_{mv}/t_{ic} \sim 1$, we have

$$\eta \cdot Oh \sim 1, \tag{5.1}$$

where $Oh = \mu/\sqrt{\rho G_s a}$ is the Ohnesorge number, which measures the relative importance of the fluid viscous force to the inertial and membrane elastic forces. Note that (5.1) is a scaling argument. From figure 9, it is seen that the transition from the overshoot–retract to the continuous-elongation mode happens when t_{mv}/t_{ic} is in the range of 0.5–1. Equation (5.1) indicates that the effect of higher capsule membrane viscosity needs to be balanced by stronger inertia (a smaller Oh), otherwise the membrane viscous effect will play the dominant role and the capsule will be in the continuous-elongation mode. This agrees with our observation from the phase diagrams of figure 9.

It is worth mentioning that the present study has assumed equal viscosity between the fluids inside and outside the capsule, and this viscosity μ has been used to normalise the membrane viscosity μ_s with $\eta = \mu_s/\mu a$. Therefore, at high η, the viscous effect that has led to the continuous-elongation mode mainly comes from the capsule membrane, and the viscous time scale is defined by the membrane viscosity.

5.2. *Practical implications of the present findings*

Here, we discuss the implications of the present results for flow experiments, in which microcapsules or biological cells are stretched by the extensional flow in the microchannel

cross-slot, and their deformation is recorded and fitted to theoretical or computational models to inversely infer the mechanical properties.

For practically unknown capsules, it is probably most convenient to carry out the experiment in the low-inertia flow regime, i.e. $Re \leq 1$, where the quasi-steady deformation mode could be observed for capsules that have been largely aligned with the centreline in the feeding channel. The quasi-steady mode, taking place near the stagnation point in the cross-slot, provides a time window of the order of $2l/U$, during which the quasi-steady shape of the capsule can be recorded. It is very encouraging to see from the present study that in case d_{oc} is below a threshold, the quasi-steady D_{XZ} of an imperfectly aligned capsule can be very close to the corresponding D_S. Therefore, it is still possible to fit the deformation to model predictions, which often only consider perfectly aligned capsules, to infer the membrane elastic properties of the capsule.

Operating experiments in the inertial flow regime is often favourable, due to the potentially much higher throughput rate, for applications that require measurement of a large-population heterogeneous capsules. However, a capsule could undergo the overshoot–retract mode of deformation, in which D_{XZ} varies quickly with time. As a result, it becomes difficult to infer mechanical properties with one instantaneous deformation profile of the capsule. In this highly unsteady mode, the maximum deformation is still a good indicator of the capsule's elasticity; however, unlike in the low-inertia flow regime, one should not directly fit the maximum deformation to model predicted steady deformation to infer properties, since the former can be considerably larger. Instead, one could use the average value of D_{XZ} when the capsule deformation is at the peak and the following trough, during the overshoot–retract deformation, which has been shown to be very close to D_S.

The present study also indicates that a capsule with a highly viscous membrane will undergo the continuous-elongation mode of deformation. One will then have to use the deformation history to infer the capsule's elasticity and viscosity. Recently, Lin *et al.* (2021) proposed such an approach, which combines a deep convolutional neural network with mechanistic capsule models, and could in principle be used for high-throughput characterisation of the membrane elasticity and viscosity of capsules flowing in a branched microchannel. However, one needs to note that direct numerical simulation of capsule deformation is often time consuming. For example, in the present study, a typical simulation took $\sim$30 hours on an HPC cluster with parallel computing using 16 cores (AMD 2.25 GHz CPU). Many hundreds of cases may be needed to build a data bank to inversely infer the mechanical properties of capsules in experiments.

We expect that the discussion above would also apply to biological cells, although the present mechanical model is still qualitative as a cell model. Indeed the model has not taken into account the cell nucleus, which could limit the cell deformation. However, these details should not qualitatively affect the balance between the flow inertia, cell elastic and viscous forces, which is the fundamental determinant of the cell's deformation mode.

6. Conclusions

The present work is the first three-dimensional computational study of the transient deformation of a viscoelastic capsule flowing through a cross-slot microchannel, focusing on the effects of the flow inertia and capsule membrane viscosity. To mimic the experimental condition that capsules or cells are often not perfectly aligned with the centreline in the feeding channel, we have considered a capsule that is released with a small initial off-centre distance. For a capsule with low membrane viscosity (e.g. $\eta \leq 2$), our

computational results show that there are mainly two modes of deformation, quasi-steady and overshoot–retract, with increasing inertial effect. At low flow inertia with $Re \leq 10$, the capsule can reach a quasi-steady state near the stagnation point of the cross-slot region, which lasts for a time period of the order $2l/U$. The quasi-steady Taylor deformation parameter is comparable to the corresponding D_S, which is the steady D_{XZ} of the same capsule released at the stagnation point. These salient features make the quasi-steady mode favourable to experiments in which a capsule's deformation profile near the stagnation point can be recorded and fitted to model predictions to inversely infer its membrane elastic properties.

With the flow inertia increasing to $Re \geq 20$, the deformation of the capsule could transit to an overshoot–retract mode, a deformation mode that has not been reported for capsules or cells in cross-slot channels. The capsule's shape oscillates, when it is passing the stagnation point, on an inertial–elastic time scale, suggesting that the dynamics is mainly driven by the balance of the flow inertial and membrane elastic forces. In this highly unsteady mode, the maximum D_{XZ} can be considerably larger than the corresponding D_S. However, interestingly, we find that the average of D_{XZ} when the capsule deformation is at the peak and the following trough is very close to D_S. Thus the average Taylor shape parameter could be calculated from experimental data and be used to infer the capsule's mechanical properties.

Regarding the effect of the capsule membrane viscosity, we find it tends to slow down the capsule deformation, postpone the onset of the maximum deformation and suppresses the overshoot–retract mode in the inertial flow regime. A highly viscous membrane, i.e. $\eta \geq 10$, can lead to a transition from the quasi-steady or overshoot–retract mode to a continuous-elongation mode, where the capsule deformation keeps increasing even when the capsule is leaving the stagnation point. The continuous-elongation mode is also a new pattern of capsule deformation in the cross-slot channel flow that is first reported in the present study. In this mode, one will need to record the deformation history of the capsule for characterisation of its elasticity and viscosity.

To conveniently predict the deformation mode of a viscoelastic capsule in the inertial flow regime, we have also proposed a scaling model, based on the competition of the inertial–elastic and membrane viscosity time scales. The model can predict the capsule deformation phase diagram reasonably well.

Supplementary movies. Supplementary movies are available at https://doi.org/10.1017/jfm.2023.298.

Acknowledgements. We are grateful for the comments of Professor C. Misbah during his visit to Queen Mary University of London (QMUL).

Funding. R.X.L. and Z.Y.G. acknowledge PhD studentships provided by QMUL and the Chinese Scholarship Council. The simulations were performed using the high-performance computer clusters of QMUL (funded by the UK EPSRC grant EP/K000128/1, EP/P020194/1 and EP/T022213/1).

Declaration of interests. The authors report no conflict of interest.

Author ORCIDs.
P. Yu https://orcid.org/0000-0003-2073-7512;
Y. Sui https://orcid.org/0000-0002-5039-9131.

References

ABAQUS/Standard Theory Manual, (Version 6.3) 2002 Hibbitt, Karlsson & Sorensen, Inc.

Armistead, F.J., De Pablo, J.G., Gadêlha, H., Peyman, S.A. & Evans, S.D. 2019 Cells under stress: an inertial-shear microfluidic determination of cell behavior. *Biophys. J.* **116** (6), 1127–1135.

BARTHÈS-BIESEL, D. & SGAIER, H. 1985 Role of membrane viscosity in the orientation and deformation of a spherical capsule suspended in shear flow. *J. Fluid Mech.* **160**, 119–135.

BOUZIDI, M., FIRDAOUSS, M. & LALLEMAND, P. 2001 Momentum transfer of a Boltzmann-lattice fluid with boundaries. *Phys. Fluids* **13** (11), 3452–3459.

CHANG, K.S. & OLBRICHT, W.L. 1993 Experimental studies of the deformation of a synthetic capsule in extensional flow. *J. Fluid Mech.* **250**, 587–608.

CORDASCO, D. & BAGCHI, P. 2017 On the shape memory of red blood cells. *Phys. Fluids* **29** (4), 041901.

DI CARLO, D., IRIMIA, D., TOMPKINS, R.G. & TONER, M. 2007 Continuous inertial focusing, ordering, and separation of particles in microchannels. *Proc. Natl Acad. Sci. USA* **104** (48), 18892–18897.

DIAZ, A., BARTHÈS-BIESEL, D. & PELEKASIS, N. 2001 Effect of membrane viscosity on the dynamic response of an axisymmetric capsule. *Phys. Fluids* **13** (12), 3835–3838.

DIMITRAKOPOULOS, P. 2014 Effects of membrane hardness and scaling analysis for capsules in planar extensional flows. *J. Fluid Mech.* **745**, 487–508.

DODSON, W.R. & DIMITRAKOPOULOS, P. 2008 Spindles, cusps, and bifurcation for capsules in Stokes flow. *Phys. Rev. Lett.* **101** (20), 208102.

DODSON, W.R. & DIMITRAKOPOULOS, P. 2009 Dynamics of strain-hardening and strain-softening capsules in strong planar extensional flows via an interfacial spectral boundary element algorithm for elastic membranes. *J. Fluid Mech.* **641**, 263–296.

EVANS, E.A. & HOCHMUTH, R.M. 1976 Membrane viscoelasticity. *Biophys. J.* **16** (1), 1–11.

EVANS, E. & YEUNG, A. 1989 Apparent viscosity and cortical tension of blood granulocytes determined by micropipet aspiration. *Biophys. J.* **56** (1), 151–160.

FISCHER, T.M. 1980 On the energy dissipation in a tank-treading human red blood cell. *Biophys. J.* **32** (2), 863–868.

GARIMELLA, R.V. & SWARTZ, B.K. 2003 Curvature estimation for unstructured triangulations of surfaces. *Tech. Rep.* LA-UR-03-8240. Los Alamos National Laboratory, Los Alamos, NM.

GIRES, P.Y., BARTHÈS-BIESEL, D., LECLERC, E. & SALSAC, A.-V. 2016 Transient behavior and relaxation of microcapsules with a cross-linked human serum albumin membrane. *J. Mech. Behav. Biomed. Mater.* **58**, 2–10.

GOSSETT, D.R., TSE, H.T.K., LEE, S.A., YING, Y., LINDGREN, A.G., YANG, O.O., RAO, J., CLARK, A.T. & DI CARLO, D. 2012 Hydrodynamic stretching of single cells for large population mechanical phenotyping. *Proc. Natl Acad. Sci. USA* **109** (20), 7630–7635.

GUCKENBERGER, A. & GEKLE, S. 2017 Theory and algorithms to compute helfrich bending forces: a review. *J. Phys.: Condens. Matter* **29** (20), 203001.

GUGLIETTA, F., BEHR, M., BIFERALE, L., FALCUCCI, G. & SBRAGAGLIA, M. 2020 On the effects of membrane viscosity on transient red blood cell dynamics. *Soft Matt.* **16** (26), 6191–6205.

GUILLOU, L., DAHL, J.B., LIN, J.M.G., BARAKAT, A.I., HUSSON, J., MULLER, S.J. & KUMAR, S. 2016 Measuring cell viscoelastic properties using a microfluidic extensional flow device. *Biophys. J.* **111** (9), 2039–2050.

GUO, Z.-L., ZHENG, C.-G. & SHI, B.-C. 2002 An extrapolation method for boundary conditions in lattice Boltzmann method. *Phys. Fluids* **14** (6), 2007–2010.

HOCHMUTH, R.M., WORTHY, P.R. & EVANS, E.A. 1979 Red cell extensional recovery and the determination of membrane viscosity. *Biophys. J.* **26** (1), 101–114.

HOLZAPFEL, G.A. 2000 *Nonlinear Solid Mechanics: A Continuum Approach for Engineering Science*. Wiley.

HU, X.-Q., SALSAC, A.-V. & BARTHÈS-BIESEL, D. 2012 Flow of a spherical capsule in a pore with circular or square cross-section. *J. Fluid Mech.* **705**, 176–194.

HYMEL, S.J., LAN, H.Z. & KHISMATULLIN, D.B. 2020 Elongation index as a sensitive measure of cell deformation in high-throughput microfluidic systems. *Biophys. J.* **119** (3), 493–501.

LI, P. & ZHANG, J.-F. 2019 A finite difference method with subsampling for immersed boundary simulations of the capsule dynamics with viscoelastic membranes. *Intl J. Numer. Meth. Biomed. Engng* **35** (6), e3200.

LI, P. & ZHANG, J. 2021 Similar but distinct roles of membrane and interior fluid viscosities in capsule dynamics in shear flows. *Cardiovascular Engng Technol.* **12** (2), 232–249.

LIN, T., WANG, Z., LU, R.-X., WANG, W. & SUI, Y. 2021 A high-throughput method to characterize membrane viscosity of flowing microcapsules. *Phys. Fluids* **33** (1), 011906.

DE LOUBENS, C., DESCHAMPS, J., BOEDEC, G. & LEONETTI, M. 2015 Stretching of capsules in an elongation flow, a route to constitutive law. *J. Fluid Mech.* **767**, R3.

DE LOUBENS, C., DESCHAMPS, J., GEORGELIN, M., CHARRIER, A., EDWARDS-LEVY, F. & LEONETTI, M. 2014 Mechanical characterization of cross-linked serum albumin microcapsules. *Soft Matt.* **10** (25), 4561–4568.

LU, R.-X., WANG, Z., SALSAC, A.-V., BARTHÈS-BIESEL, D., WANG, W. & SUI, Y. 2021 Path selection of a train of spherical capsules in a branched microchannel. *J. Fluid Mech.* **923**, A11.

MALEKI, M., DE LOUBENS, C., XIE, K.-L., TALANSIER, E., BODIGUEL, H. & LEONETTI, M. 2021 Membrane emulsification for the production of suspensions of uniform microcapsules with tunable mechanical properties. *Chem. Engng Sci.* **237**, 116567.

PESKIN, C.S. 2002 The immersed boundary method. *Acta Numer.* **11**, 479–517.

POZRIKIDIS, C. & JANKOWSKI, D. 1997 *Introduction to Theoretical and Computational Fluid Dynamics*, vol. 675. Oxford University Press.

RAMANUJAN, S. & POZRIKIDIS, C. 1998 Deformation of liquid capsules enclosed by elastic membranes in simple shear flow: large deformations and the effect of fluid viscosities. *J. Fluid Mech.* **361**, 117–143.

SKALAK, R., TOZEREN, A., ZARDA, R.P. & CHIEN, S. 1973 Strain energy function of red blood cell membranes. *Biophys. J.* **13** (3), 245–264.

SUI, Y., CHEW, Y.-T., ROY, P. & LOW, H.-T. 2008 A hybrid method to study flow-induced deformation of three-dimensional capsules. *J. Comput. Phys.* **227** (12), 6351–6371.

TRAN-SON-TAY, R., SUTERA, S.P. & RAO, P.R. 1984 Determination of red blood cell membrane viscosity from rheoscopic observations of tank-treading motion. *Biophys. J.* **46** (1), 65–72.

WALTER, A., REHAGE, H. & LEONHARD, H. 2000 Shear-induced deformations of polyamide microcapsules. *Colloid Polym. Sci.* **278** (2), 169–175.

WANG, Z., SUI, Y., SALSAC, A.-V., BARTHÈS-BIESEL, D. & WANG, W. 2016 Motion of a spherical capsule in branched tube flow with finite inertia. *J. Fluid Mech.* **806**, 603–626.

WANG, Z., SUI, Y., SALSAC, A.-V., BARTHÈS-BIESEL, D. & WANG, W. 2018 Path selection of a spherical capsule in a microfluidic branched channel: towards the design of an enrichment device. *J. Fluid Mech.* **849**, 136–162.

WATKINS, N., VENKATESAN, B.M., TONER, M., RODRIGUEZ, W. & BASHIR, R. 2009 A robust electrical microcytometer with 3-dimensional hydrofocusing. *Lab on a Chip* **9** (22), 3177–3184.

YAZDANI, A. & BAGCHI, P. 2012 Three-dimensional numerical simulation of vesicle dynamics using a front-tracking method. *Phys. Rev.* E **85** (5), 056308.

YAZDANI, A. & BAGCHI, P. 2013 Influence of membrane viscosity on capsule dynamics in shear flow. *J. Fluid Mech.* **718**, 569–595.

ZHONG-CAN, O.-Y. & HELFRICH, W. 1989 Bending energy of vesicle membranes: general expressions for the first, second, and third variation of the shape energy and applications to spheres and cylinders. *Phys. Rev.* A **39** (10), 5280.